Chemical Science

ROYAL SOCIETY OF CHEMISTRY

EDGE ARTICLE

View Article Online
View Journal

Cite this: DOI: 10.1039/d5sc08281a

All publication charges for this article have been paid for by the Royal Society of Chemistry

Stepwise functionalization-induced molecular tweak unveiling multi-level thermochromic data encryption and fingerprint monitoring system

Debika Barman, [a] Retwik Parui [a] and Parameswar Krishnan Iyer *[ab]

Protecting hierarchical data *via* multi-level encryption and authenticating high-contrast touch traces represents an emerging frontier demanding technological innovation in molecular materials. Herein, *via* precise molecular interventions, three D–A–A′ (donor–acceptor–acceptor) type aggregation induced emission (AIE)-active positional isomers (*p*-TPy, *m*-TPy, and *o*-TPy) are designed by varying the pyridine ring position in the acceptor. Their systematic investigation reveals key photophysical and structure–property insights, revealing their potential in advanced security and encryption. Positional modulation regulates electron-accepting strength and molecular packing, leading to red-shifted solid-state emission and influencing PLQY, transient PL, solvatochromism, and thermal stability as supported by crystal analysis and theoretical calculations. These stimuli-adaptive isomers address two critical challenges in advanced security systems. First, thermochromic luminescent materials (TLMs) exhibiting multiple temperature-dependent luminescent states are formulated as security inks by doping the *para*-isomer into phase-change matrices, enabling a multi-level security system. Second, a red-emissive, water-soluble amphiphilic fluorescent probe is obtained by functionalizing the *para*-isomer into a pyridinium emitter (*p*-TPyMe), capable of detecting latent fingerprints on diverse substrates and revealing level-3 ridge details with an exceptional contrast value of 5.39. These results demonstrate how molecular design in single chromophores translates into strategic AIE-active stimuli-adaptive positional isomers with intricate structure–property relationships, highlighting their potential for next-generation anti-counterfeiting, data encryption, and forensic technologies.

Received 26th October 2025
Accepted 2nd March 2026

DOI: 10.1039/d5sc08281a

rsc.li/chemical-science

Introduction

Metal-free organic π-conjugated molecules offer advantages of precise tunability to achieve desired structural modifications, and have found wide-ranging applications in areas such as security inks and data encryption,[1] fingerprint detection,[2] switches,[3] and sensors.[4] In general, materials incorporating an electron donor (D) and acceptors (A) connected *via* a conjugated bridge are preferred, as their inherently twisted molecular architectures increase the likelihood of exhibiting aggregation-induced emission (AIE) characteristics.[5] The optical and electrical properties of those emitters are strongly influenced by both the molecular structure and their solid-state structural organization, with emission largely dictated by molecular conformation and non-covalent interactions.[6,7] However, previous studies have primarily focused on the effects of the type and number of substituents on the photophysical properties of PL materials. It is well established that the position of substituents significantly influences the photophysical properties of isomers.[8,9] Despite having identical functional groups, slight variations in their substitution positions can lead to distinct molecular arrangements, which in turn alter the electron affinity, ionization potential, electronic absorption, fluorescence spectra, and dipole moment, resulting in new materials with intriguing optoelectronic properties.[10–13] Likewise, a recent study has demonstrated that by altering the position of cyano groups within the π-conjugated backbone of styrylbenzene molecules significantly influences their solid-state luminescence.[14] Despite its huge significance, the impact of isomerization on the fluorescence behavior of organic fluorophores in the solid state has been addressed in only a handful of discrete reports.[15–17] Thus, comprehensive studies aimed at understanding the structure–property relationships are essential for the rational design and development of novel molecules with tailored photophysical properties, even at harsh temperature conditions for very specific applications.

This conformational sensitivity of AIEgens can be further harnessed to develop smart luminescent materials, particularly thermo-responsive materials, enabling their advanced applications in areas such as anti-counterfeiting,[18] information encryption and decryption,[19] and other high security-related

[a]Department of Chemistry, Indian Institute of Technology Guwahati, Guwahati 781039, India. E-mail: pki@iitg.ac.in
[b]Centre for Nanotechnology, Indian Institute of Technology Guwahati, Guwahati 781039, India

technologies based on their thermochromic behavior. Thermochromic luminescent materials (TLMs) are developed either by leveraging the inherent temperature-responsive properties of luminescent materials or by incorporating high-contrast AIEgens into phase-change polymer matrices. However, achieving TLMs capable of exhibiting more than two luminescent states at varying temperatures remains very challenging, especially high-contrast red emitting, due to the lack of effective and rational design strategies.

To mitigate the multiple issues outlined above, we have designed a series of D–A–A′-based AIE active positional isomers, *i.e.*, *p*-TPy, *m*-TPy, and *o*-TPy, by varying the position of the pyridine ring within the acceptor moiety, aiming to explore the structure–property relationships arising from conformational changes (Scheme 1). Upon modulating the position of the pyridine unit with respect to the phenyl bridge is expected to affect the electron-accepting strength and alter the molecular packing characteristics of the isomers. A comparative investigation into how positional variation affects the solid-state photophysical behavior, AIE characteristics, photoluminescence quantum yield (PLQY), solvatochromism, transient PL, and viscosity dependence of the isomers has been conducted, with findings supported by crystal structure analysis and theoretical calculations. Conceptually, the *para* isomer, *p*-TPy, was utilized for the design of a thermochromic luminescent material (TLM) by embedding it into the thermoplastic polymer, PEG. Three distinct TLM security inks exhibiting unique thermochromic transition temperatures were developed by incorporating the *p*-TPy isomer into PEG2000, PEG4000, and PEG20000 matrices. This strategy facilitates the development of security inks with tailored thermal response behaviors, thereby improving their utility for multi-level data encryption and authentication systems. Therefore, the development of TLMs with tunable response behaviors is of great scientific and industrial importance for constructing advanced, multilevel anti-counterfeiting security systems.

Additionally, condensed state luminogens exhibiting amphiphilic behavior are extremely rare and can serve as ideal candidates for sensitive touch traces such as latent fingerprint (LFP) detection owing to their easy functionalization, high contrast, and intrinsic AIE characteristics.[20,21] Moreover, developing a water-soluble AIE developer that does not rely on organic solvents is a major strategic step forward since it is easier to prepare, and exhibits a fluorescence turn-on mode with longer-wavelength emission to enhance resolution and contrast, which are very rare and of significant importance. Drawing motivation from these challenges, the free nitrogen atom in the pyridine core of the *para* isomer (*p*-TPy) was employed to transform the lipophilic AIEgen into an amphiphilic pyridinium salt, *p*-TPyMe. This strategic modification furnished a water-soluble, amphiphilic emitter, purposefully tailored for high-performance LFP detection, delivering an impressive contrast value of 5.39 and enabling precise forensic analysis. The fluorophore exhibits excellent LFP development performance through a fluorescence turn-on mechanism at longer wavelength emission, providing up to level 3 details and a very high contrast ratio, achieved simply by the immersion method in an aqueous *p*-TPyMe solution, without the need for any organic cosolvent or further processing. This level of precision paves the way for highly accurate fingerprint touch trace identification, making it the most powerful and convenient tool for forensic science available presently.

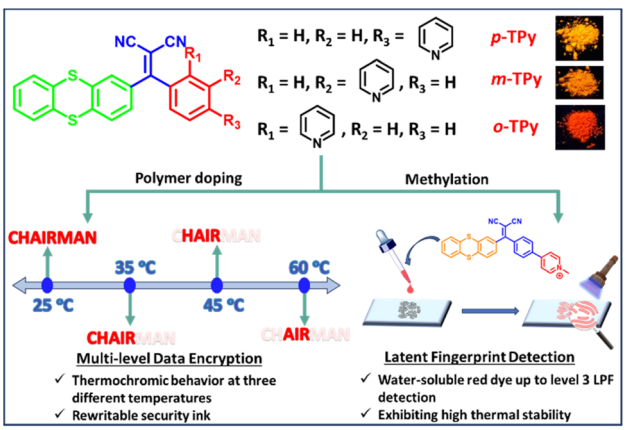

Scheme 1 Chemical structures of the investigated positional isomers and a schematic illustration of their application in multi-level anti-counterfeiting and latent fingerprint detection after respective modification.

Results and discussion

The D–A–A′ type positional isomers, *p*-TPy, *m*-TPy, and *o*-TPy, were rationally designed and synthesized to systematically investigate how variation in the attachment position of the pyridine unit on the bridging phenyl ring influences the photophysical properties. In this molecular framework, thianthrene was employed as a twisted electron donor to suppress excessive π–π stacking and promote structural distortion, while malononitrile and pyridine functioned as dual acceptor units to construct a D–A–A′ architecture with enhanced intramolecular charge-transfer (ICT) sensitivity. By solely altering the positional linkage of the pyridine moiety (*para*, *meta*, or *ortho*) without changing the molecular composition, precise regulation of conjugation efficiency, molecular conformation, and solid-state packing can be achieved. This positional isomer engineering strategy enables a clear elucidation of structure–property relationships and excited-state modulation in D–A–A′ systems. The target molecule was obtained *via* a three-step synthetic procedure, *viz.*, Friedel–Crafts acylation, Suzuki cross-coupling, and Knoevenagel condensation reaction. The synthetic pathway for the position isomers is outlined in Scheme S1. ^{1}H NMR, ^{13}C NMR, and HRMS analyses were conducted carefully to characterize all the obtained products (Fig. S1–S11).

Unveiling the photophysical behavior of the positional isomers

The pyridine unit was linked to the three different positions of the phenyl ring, anchored with a malononitrile group, resulting in the formation of the *para* (*p*-TPy), *meta* (*m*-TPy), and *ortho* (*o*-TPy) isomers, respectively. Since the position of the substituent

was believed to have a significant impact on the photophysical properties of the isomers, detailed photophysical studies were conducted in solution, aggregated, and solid states. The isomers exhibit two prominent absorption bands: one in the lower wavelength region (300–350 nm) attributed to π–π* transitions, and another in the higher wavelength region (390–425 nm) corresponding to intramolecular charge transfer (ICT) transitions between the donor and acceptor functionality (Fig. S12a). The isomers exhibit emission maxima within the range of 550–700 nm in their aggregated state, with *m*-TPy and *o*-TPy displaying a slight blue-shifted emission compared to *p*-TPy due to reduced conjugation caused by its highly twisted structure (Fig. S12b).

The ICT transition is highly sensitive to solvent polarity changes and serves as a defining characteristic of donor–acceptor molecules. These synthesized compounds were anticipated to exhibit pronounced charge transfer behavior due to the D–A–A'type architecture. The solvatochromic study was conducted by varying the solvents from non-polar (hexane) to polar solvent (methanol) while maintaining a constant luminogen concentration (50 μM) in UV-visible and PL experiments. Minimal change in absorption bands was observed for all the isomers on changing the solvent polarity from non-polar to polar, indicating that the variations in environmental polarity had minimal impact on the ground-state electronic structures (Fig. S12c–e). Interestingly, for all isomers, an increase in solvent polarity from hexane to methanol resulted in a notable red shift in the emission spectrum along with a decrease in intensity. Specifically, the emission peaks shifted significantly from 586 to 654 nm (68 nm) for *p*-TPy, 585 to 644 nm (59 nm) for *m*-TPy, 582 to 637 nm (55 nm) for *o*-TPy (Fig. 1a–c). However, the emission intensity of all isomers is completely suppressed in highly polar solvents such as methanol, DMF, DMSO, and acetonitrile. This suppression is attributed to the formation of a twisted intramolecular charge transfer (TICT) state, which leads to a continuous redshift and a decrease in emission intensity. In polar environments, the excited charge-transfer state is significantly stabilized, which promotes conformational twisting between the donor and acceptor moieties, generating a TICT state with reduced orbital overlap. This twisted geometry facilitates non-radiative decay pathways, thereby quenching fluorescence. Interestingly, the *para* isomer (*p*-TPy) exhibited a greater redshift in its emission maxima compared to the *meta* and *ortho* isomers, suggesting the involvement of extended π-conjugation in the *p*-TPy, which enhances donor–acceptor electronic communication and strengthens the ICT character, making it more sensitive to solvent polarity.

Conventionally, the twisted architecture of the isomers facilitates aggregation-induced solid-state emission. To further investigate this behavior, a fluorescence experiment was conducted using DMF as a good solvent and water as a poor solvent. Nanoaggregate formation was triggered by gradually adding water to the DMF solution, and the AIE characteristics of the isomers were evaluated through fluorescence measurements. Negligible variation in the fluorescence intensity was observed with increasing the water fraction (f_w) from 0% to 70% in DMF/water mixture (Fig. 1d and S13a–c). However, a sharp increase in emission intensity was observed as f_w further increased to 80% and reached the maximum value at f_w 99%, 90%, and 99%, resulting in an orange emission peaked at 610 nm, 605 nm, and 605 nm for *p*-TPy, *m*-TPy, and *o*-TPy, with a photoluminescence

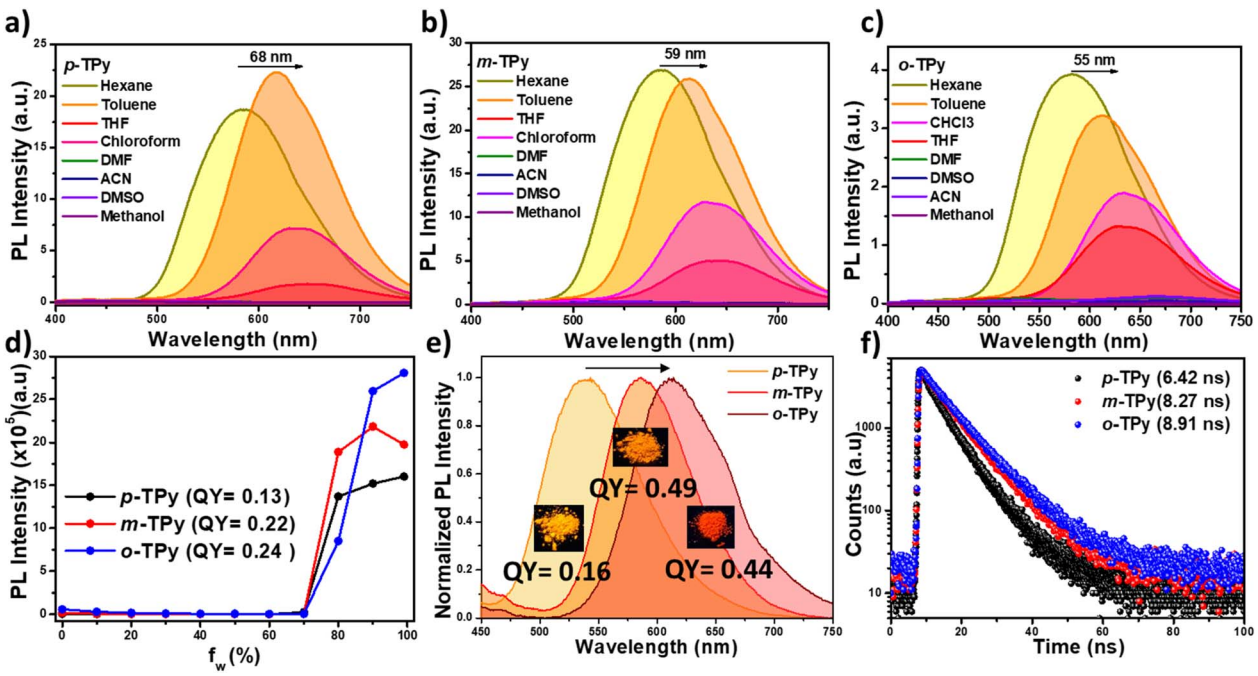

Fig. 1 Emission spectra of the isomers (a) *p*-TPy, (b) *m*-TPy and (c) *o*-TPy recorded in solvents with varying polarities. (d) Plot of fluorescence intensity *versus* water fraction (% f_w); luminogen concentration: 50 μM, with intensity measured at λ_{max}. (e) Solid-state PL spectra of *p*-TPy, *m*-TPy, and *o*-TPy, accompanied by photographs under 365 nm UV illumination. (f) Transient PL decay profiles of *p*-TPy, *m*-TPy, and *o*-TPy in their solid state.

quantum yield (PLQY) of 13%, 22% and 24% respectively (Fig. 1d and S13a–c). These findings suggest that all the isomers exhibit a distinct AIE property due to the restriction of intramolecular motion (RIM). The nano aggregate formation of the isomers was further visualized *via* FESEM analysis. Fig. S13d–f illustrate the formation of nano aggregates with square, spherical, and rectangular shapes for *p*-TPy, *m*-TPy, and *o*-TPy, respectively, within the 200–250 nm size range.

To interpret the role of the functional group position, solid-state emission properties of the isomers were recorded for powder samples. Unlike aggregate state, all the isomers exhibited distinct emission properties in their solid state. The fluorescence spectrum of *p*-TPy exhibited a blue-shifted emission peak at approximately 560 nm in the solid state compared to its aggregated state (Fig. 1e). This 50 nm blue shift in the λ_{max} of *p*-TPy is substantial enough to change its emission color from orange to yellow, with CIE coordinates of (0.56, 0.43) for the solid state and (0.35, 0.53) for the aggregated state (Fig. 1e, S14a and b). Similarly, for *m*-TPy, the solid-state emission spectrum was shifted by 25 nm towards lower wavelength compared to its aggregated state, with λ_{max} values of 580 nm and 605 nm for the solid and aggregated states, respectively, and corresponding CIE coordinates were (0.45, 0.39) and (0.55, 0.44) (Fig. 1e, S14a and b). In contrast, *o*-TPy showed an emission maximum at 612 nm, consistent with its nanoaggregate emission behavior, with CIE coordinates of (0.54, 0.37) in the solid state and (0.55, 0.44) in the aggregated state. Also, the quantum yields of the isomers are highly affected by slight changes in their conformation, followed by modulation in the position of the pyridine group. The quantum yields for *p*-TPy, *m*-TPy, and *o*-TPy in their solid state are 16%, 49% and 44%, respectively (Fig. 1e). Additionally, the positional isomers also displayed a distinct average lifetime of 6.42 ns, 8.27 ns and 8.91 ns for the *p*-TPy, *m*-TPy, and *o*-TPy in their solid states, respectively (Fig. 1f).

Structural elucidation *via* single crystal XRD

The distinct photophysical properties of the positional isomers are likely attributed to the differences in their solid-state packing. To further investigate these differences in molecular packing, single-crystal analysis was performed. We successfully obtained well-diffracted single crystals for *m*-TPy and *p*-TPy and compared their conformational differences to reveal the disparities in their condensed state optical phenomena. Yellow and orange-colored crystals were obtained through the slow evaporation method using a mixture of chloroform and hexane as solvents. However, despite repeated attempts using various crystal growth techniques, suitable well-diffracting single crystals of *o*-TPy for SCXRD analysis were not obtained. Both *p*-TPy and *m*-TPy crystallize in the monoclinic with space group *P*21/*n*.

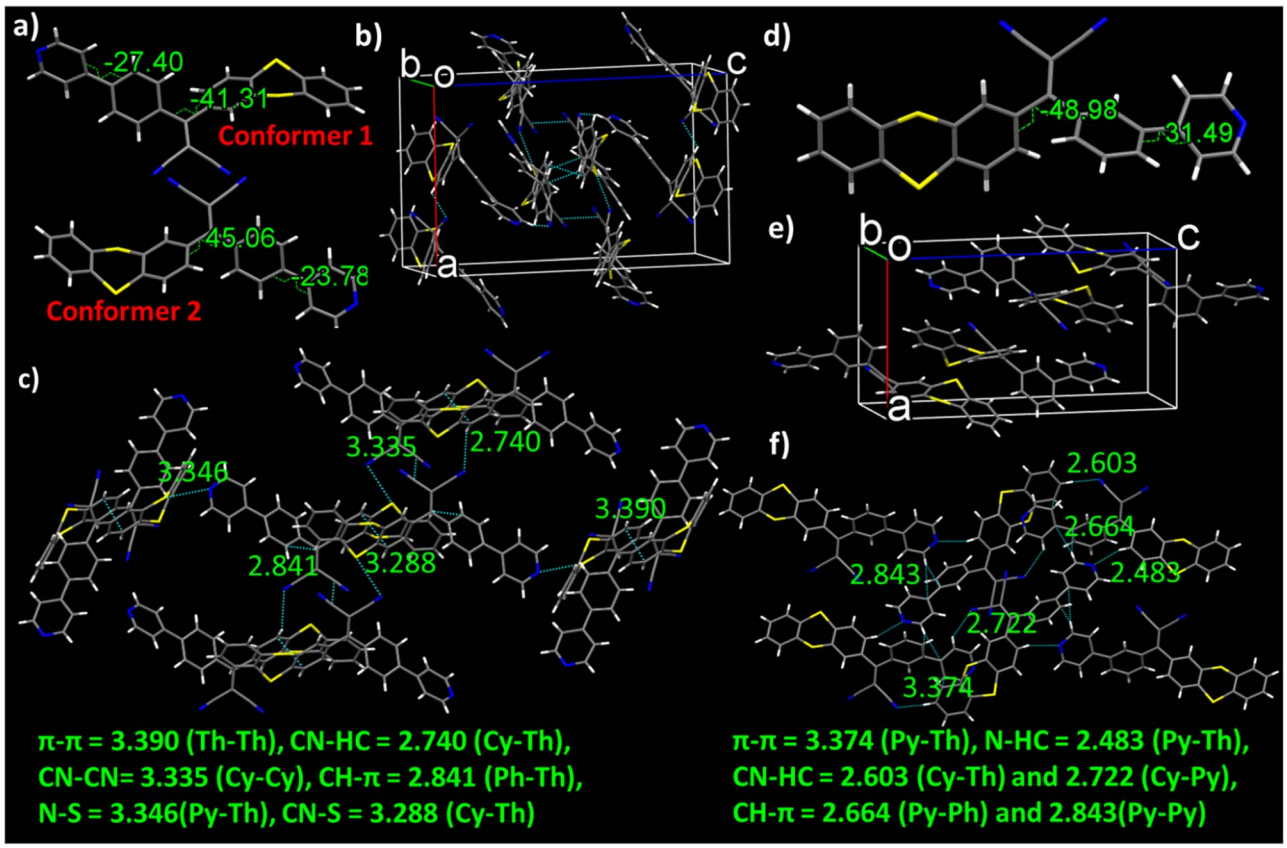

Fig. 2 Molecular conformation of *p*-TPy (a) and *m*-TPy (d) in the crystal lattice. Detailed views of Intermolecular interactions and molecular packing in the crystal lattice of (b and c) *p*-TPy and (e and f) *m*-TPy, demonstrating the distinct packing motifs and interaction patterns arising from its structural isomerism.

In case of *p*-TPy, two conformers with different twist angles and interactions coexist as a dimer within the same crystal packing. By analyzing the angle between the thianthrene (Th) core and the malononitrile (MN) unit, we observed twist angles of 41.31° and 45.06° between the donor and acceptor groups for conformers 1 and 2, respectively (Fig. 2a). Similarly, the twist angles between the pyridine (Py) unit and the bridging phenyl ring (Ph) were measured at 27.40° for conformer 1 and 23.78° for conformer 2, highlighting the unique twisting characteristics of each conformer. Furthermore, conformer 1 exhibited six non-covalent interactions with neighbouring molecules, whereas conformer 2 showed only four (Fig. 2a). Notably, the N···S (3.346 Å) and CH···π (2.841 Å) interactions observed in conformer 1 were absent in conformer 2 (Fig. 2c). Each conformer forms a dimer with its own type and is arranged in a segregated stacking pattern in the crystal packing (Fig. S14c). As anticipated, the *meta* isomer, *m*-TPy, adopts a more twisted structure than the *para* isomer, with twist angles of 48.98° and 31.49° between the thianthrene–malononitrile unit and the pyridine–phenyl group, respectively (Fig. 2d). Notably, only one conformer is observed in the crystal packing. Likewise, *m*-TPy engaged in six distinct non-covalent interactions with neighboring molecules, including an N···HC hydrogen bond (2.483 Å) (Fig. 2e and f). Overall, the single-crystal analysis clearly suggests that *m*-TPy adopts a more twisted donor–acceptor architecture and a distinct packing arrangement compared to *p*-TPy, and these structural variations directly modulate the extent of intramolecular charge transfer and molecular rigidity in the solid state, thereby leading to their different emission colors.

Interestingly, in the aggregate and amorphous states, both isomers exhibited red-shifted emission maxima around 610/605 nm compared to their crystalline states (560 nm for *p*-TPy and 590 nm for *m*-TPy) (Fig. S15a). This red shift in the aggregated state can be attributed to the TICT effect induced by the polar aqueous environment. In contrast, the well-defined molecular packing in the crystalline state restricts the TICT effect, resulting in relatively blue-shifted emission. Additionally, the PLQY values were higher in the crystalline state (0.18 for *p*-TPy and 0.48 for *m*-TPy) compared to the aggregated state (0.13 and 0.22, respectively), confirming that molecular packing significantly influences both emission wavelength and efficiency. The slightly blue-shifted emission of *p*-TPy compared to *m*-TPy can be attributed to the more twisted molecular structure of *m*-TPy. This increased twist in *m*-TPy leads to a stronger TICT effect, resulting in a red-shifted emission maximum relative to *p*-TPy. Furthermore, the powder X-ray diffraction (PXRD) patterns of the isomers showed precise alignment with simulated data generated from SC-XRD analysis, demonstrating the exceptional crystallinity of the powdered samples (Fig. S15b–d).

DFT-based interpretation of molecular behavior

To validate the impact of structural modulation on electronic distribution, density functional theory (DFT) calculations were performed. A slight increment in the HOMO–LUMO energy bandgap was observed, from 3.21 eV to 3.28 eV, as the pyridine group shifted from the *para* to the *ortho* position (Fig. S16a–c). In all the isomers, the HOMO electron cloud is localized on the thianthrene core. However, for the *para* isomer, *p*-TPy, the LUMO electron cloud extends across the entire acceptor group, including both malononitrile and pyridine group. In contrast, for the *m*-TPy and *o*-TPy isomers, the LUMO electron cloud is confined to the malonitrile group due to conjugation disruption and steric hindrance. Moreover, the shift of the pyridine group from the *para* to the *meta* and *ortho* positions significantly influences the conformational twist in the DFT-optimized structures, resulting in an increase in the dihedral angle between the thianthrene–malononitrile unit (42.85°, 43.39°, 60.76°) and the pyridine–phenyl group (38.45°, 40.13°, 51.77°) for *p*-TPy, *m*-TPy and *o*-TPy respectively (Fig. S16d–f). In the solid state, the emission spectrum of *o*-TPy exhibited a more pronounced red shift compared to *m*-TPy, which was itself more red-shifted than *p*-TPy (λ_{max} *p*-TPy < *m*-TPy < *o*-TPy). This trend can be attributed to enhanced charge transfer (CT) associated with the increased twist angle as the pyridine position shifts from *para* to *ortho*.[22]

Viscosity-driven photophysical transitions

Molecular rotors are fluorescent probes sensitive to the nature of their environment, as their emissive properties occur through the restriction of intramolecular rotation and vibration. Looking into the twisted rotor-like architecture of the isomers, we investigated their viscosity-dependent fluorescence behavior using a water-glycerol mixture. As the viscosity of the medium increased, the fluorescence intensity of the isomers decreased at around 600 nm with the simultaneous emergence of a new peak at 430 nm (Fig. S17a–c). In 100% glycerol, the intense peak at 600 nm was fully quenched, while a weaker peak appeared at 430 nm. This quenching of emission intensity is likely due to the disruption of aggregate formation in the glycerol medium, whereas the new peak at 430 nm is attributed to monomeric emission resulting from the slight restriction of molecular motion in the highly viscous environment.

Thermal stability

To further understand the thermal behavior, DSC and TGA analyses were performed of the four luminogens (Fig. S17d and e). The DSC thermograms exhibit broad endothermic transitions in the range of 130–260 °C, which are attributed to a phase transition (Fig. S17e). Additionally, TGA analysis demonstrates a slight weight loss observed below 350 °C, which can be attributed to the removal of physically adsorbed moisture or residual solvent molecules (Fig. S17d). The major thermal decomposition occurs at significantly higher temperatures, confirming the excellent thermal stability of the luminogens.

Thermochromic luminescent material (TLM) for data encryption

After gaining a thorough understanding of how various non-covalent intermolecular interactions influence the photophysical properties of the isomers in varying environments, we further explored their development as stimulus-responsive luminescent materials and formulations. The *p*-TPy isomer was chosen for the preparation of a thermochromic

luminescent material (TLM) owing to its higher synthetic accessibility and pronounced ICT characteristics, which makes it particularly suitable for thermochromic modulation. It was subsequently embedded into the widely used thermoplastic polymer PEG as the matrix (Fig. 3a). As illustrated in Fig. 3b, the emission band at 610 nm, displaying bright orange fluorescence, diminishes at 35 °C and eventually becomes non-emissive. Once the temperature returned to room temperature, the emission color reversed from non-emissive to bright orange. Typically, upon heating, the internal micro-environment of the PEG matrix undergoes changes due to increased free volume and enhanced polymer chain mobility. This alteration is sufficient to disrupt the intermolecular interactions and aggregate formation, ultimately leading to emission quenching. As depicted in Fig. 3c, the temperature-dependent PL spectral changes of *p*-TPy/PEG2000 were repeatedly recorded at room temperature and 35 °C over ten consecutive cycles without any significant intensity variations, confirming that the prepared TLM exhibited excellent reversibility.

Strengthening the security of data encryption inks has become a significant challenge due to the increasing incidents of document forgery and counterfeiting. Consequently, there is a high demand for the development of multi-level data encryption inks. In this regard, the variation in phase transition temperatures among PEGs with different molecular weights was employed to

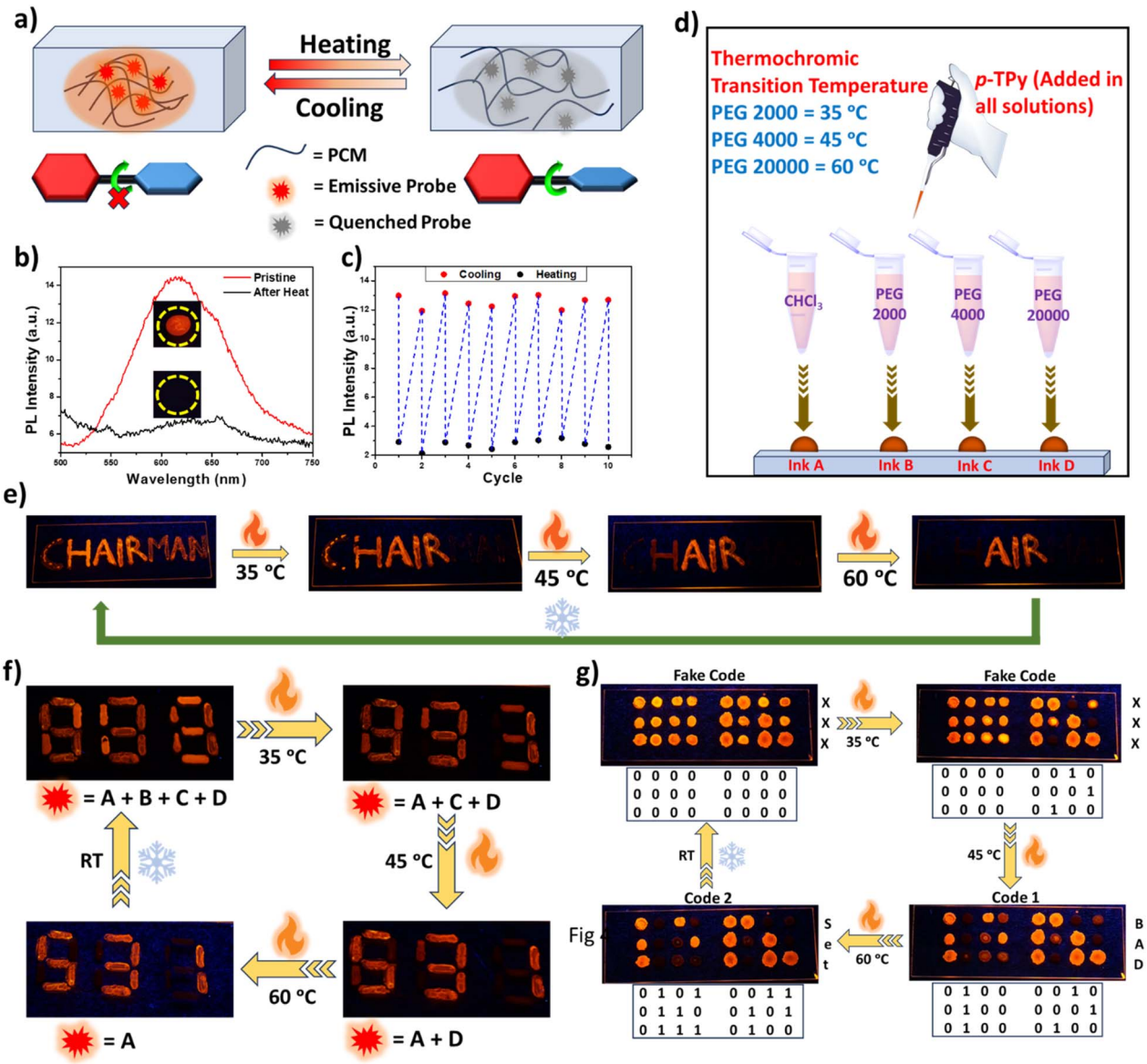

Fig. 3 (a) Schematic illustration of thermochromic luminescence arising from reversible aggregation and disaggregation triggered by heating and cooling. (b) Temperature-dependent emission spectra of *p*-TPy/PEG2000 recorded during heating from 25 °C to 35 °C. (c) Demonstration of thermal cycling stability/intensity variations measured over ten consecutive heating–cooling cycles from 25 °C to 35 °C. (d) Preparation of thermochromic luminescent inks using *p*-TPy and phase change matrix, PEG. Photographs of luminescent letters (e), digital number (f) and binary code (g) written with four different TLM encryption inks, recorded under 365 nm UV light before and after heating.

design a series of TLMs with particular thermochromic transition temperatures. Three different TLM security inks with unique thermochromic transition temperatures were obtained by incorporating *p*-TPy isomer into PEG2000, PEG4000, and PEG20000 matrices at 2.5 wt% (Fig. 3d). Varying the molecular weight of PEG enabled fine-tuning of the thermochromic transition temperature of each ink precisely, since the melting point and phase-transition characteristics of PEG rise with increasing molecular weight. To further validate the use of these TLMs as security ink for multi-level anti-counterfeiting, we utilized the *p*-TPy isomer solution (Ink A) along with TLMs based on *p*-TPy/PEG2000 (Ink B), *p*-TPy/PEG4000 (Ink C), and *p*-TPy/PEG20000 (Ink D) composites to inscribe the letters AIR, MAN, C, and H on glass substrates, respectively, forming the word "CHAIRMAN" (Fig. 3e). All letters exhibited an orange glow at room temperature. Upon heating to 35 °C, the orange fluorescence of the letters 'MAN' transitioned from emissive to non-emissive, while the remaining letters retained their glow, forming the word "CHAIR". At 45 °C, the letter 'C' transitioned from emissive to non-emissive and generated another word "HAIR". When the glass substrate was heated to 60 °C, the orange emission of the letter 'H' also became non-emissive. The letters 'AIR' remained unchanged, as they were written using only the *p*-TPy solution. Once the glass substrate returned to room temperature, all letters regained their original orange glow and displayed the initial letter "CHAIRMAN".

Similarly, a reversible multi-encryption and decryption strategy was devised to further explore the potential application of TLM inks in optical encoding. In the first experiment, the numerical code '888' was inscribed on a glass slide using three TLM inks and the *p*-TPy isomer solution (Fig. 3f). At room temperature, all digits exhibited bright orange fluorescence. As the temperature increased to 35 °C, the code transformed from '888' to '893'. Further heating to 45 °C altered it to '691', and at 60 °C, it changed to '531'. However, upon returning to room temperature, the code reverted back to '888'. In the second experiment, orange fluorescent TLMs were used as encryption ink, while an isomer fluorescent solution served as a stable ink to write a binary code designed to prevent information leakage. As shown in Fig. 3g, under UV light at room temperature, the binary code was intentionally misrepresented. Even at 35 °C, a false code appeared to provide misinformation for enhanced security encryption. However, when the glass slide was heated to 45 °C, the first part of the security code clearly appeared, followed by the appearance of the second part of the code after the temperature increased to 60 °C. Upon returning to room temperature, the code was erased once again. Interestingly, our data encryption and decryption strategy allowed us to store different information that could be revealed at different temperatures. As a result, only authorized individuals who are aware of the correct encryption methods and the precise heating temperature can access the hidden information, significantly enhancing the security of the protected data. Based on the above results, the TLMs developed in this work demonstrated greater suitability for multi-level encryption strategies and advanced confidential information protection systems compared to previously reported encryption methods.

Fluorescence-based detection of latent fingerprints

Furthermore, exploiting the nucleophilic character of the pyridine nitrogen in the *para* isomer (*p*-TPy), it was modified to enhance hydrophilicity by quaternizing the pyridine nitrogen, yielding a pyridinium salt (Fig. 4a). The combination of a hydrophilic pyridine cation and lipophilic thianthrene units renders *p*-TPyMe amphiphilic, making it soluble in water as well as in polar organic solvents such as acetone, methanol, ethanol, acetonitrile, DMSO, DMF, and THF. Upon excitation at 430 nm, the emitter exhibited red emission with a maximum wavelength at 720 nm in its solid state (Fig. S18a and b). Due to its water solubility, high-contrast red emission, and amphiphilic nature of *p*-TPyMe, we utilized the emitter for fingerprint identification. The development of latent fingerprints (LFP) using fluorescence molecules involves two approaches: the powder dusting method and the solution method. Among these, the solution method is more widely studied due to its simplicity and low dye consumption. To assess the effectiveness of *p*-TPyMe in LFP development, a fingerprint on aluminum foil was immersed in an aqueous *p*-TPyMe solution at varying concentrations for 1 minute (Fig. 4b). At a lower concentration of 10 μM, the fingerprint profile appeared faint and indistinguishable, but it became distinctly visible at concentrations exceeding 30 μM. Under 375 nm light irradiation, bright red and high-quality fluorescence images of LFPs were observed, resulting from the preferential accumulation of *p*-TPyMe on the fingerprint ridges rather than the furrows due to the absence of sweat secretion (Fig. 4c). FESEM images reveal a preferential accumulation of *p*-TPyMe on the fingerprint ridges compared to the furrows (Fig. S18c).

To investigate the LFP development mechanism or identify which component in LFPs interacts with *p*-TPyMe, the letters "LFP" were inscribed on aluminum foil using aqueous solutions of key LFP components, including glucose, glycine, sodium chloride, lysine, lactic acid, and oleic acid. The dried inscriptions were soaked in a 50 μM aqueous solution of *p*-TPyMe. Upon exposure to a 375 nm lamp, only the letters inscribed with oleic acid exhibited a vivid red fluorescence and remained clearly distinguishable, confirming the probe's ability to stain oleic acid in the LFPs (Fig. 4d). To further confirm the mechanism responsible for the red emission, the emission spectra of *p*-TPyMe were recorded in various solvents, including hexane, toluene, diethyl ether, methanol, ethanol, acetone, and water, as well as oleic acid. As shown in Fig. S18d, *p*-TPyMe exhibited no significant emission in any of the tested solvents except oleic acid, where a distinct peak appeared at 640 nm, accounting for its red emission. These results confirmed the selective interaction of *p*-TPyMe with oleic acid over other polar and non-polar solvents, thereby also demonstrating its amphiphilic nature. The red emission observed from *p*-TPyMe upon interaction with oleic acid is likely attributed to AIE through restriction of intramolecular motion (RIM), promoted by the high supramolecular assembly in oleic acid (Fig. 4c). To further verify this, PL spectra were recorded by incrementally adding oleic acid to an aqueous solution of *p*-TPyMe at concentrations ranging from 0.05% to 0.25%, with a spectrum measured after each addition.

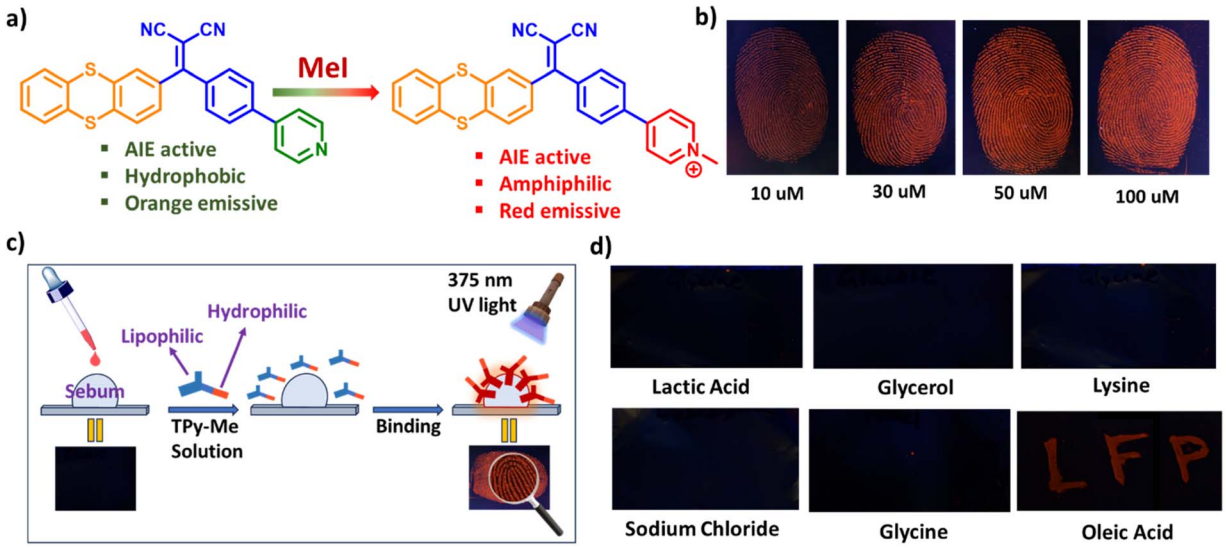

Fig. 4 (a) Synthetic pathway illustrating the structural transformation of a lipophilic AIEgen (*p*-TPy) into its amphiphilic AIEgen (*p*-TPyMe). (b) Fluorescence images of LFP developed with an aqueous solution of *p*-TPyMe with different concentrations under 375 nm light. (c) Diagram depicting the mechanism of LFP formation with *p*-TPyMe in aqueous solution. (d) Fluorescence images of the characters 'LFPs' written using various substances commonly found in LFPs and treated with a *p*-TPyMe aqueous solution (50 μM).

A significant enhancement in fluorescence intensity was observed, which suggests a strong interaction between *p*-TPyMe and oleic acid, likely due to aggregation that restricts non-radiative decay, consistent with AIE-like behavior. This property enables efficient detection of LFPs in the presence of oleic acid.

High-resolution LFPs were successfully developed, displaying clear level 1–3 fingerprint details using *p*-TPyMe, without any additional optical, thermal, or chemical treatment. Typically, fingerprint analysis involves three levels: level 1 includes general ridge patterns such as cores and lakes; level 2 encompasses features like ridge endings, short ridges, and bifurcations; and level 3 involves fine, quantitative details such as ridge path deviations, sweat pores, and ridge contours. Level 1 fingerprint features are clearly visible on the substrates; however, they lack the uniqueness required for definitive individual identification (Fig. 5a). Therefore, detailed fingerprint analysis at levels 2 and 3 was conducted on aluminum foil. As illustrated in Fig. 5a, the magnified local images clearly reveal ridge endings, bifurcations, and short ridges (level 2), along with sweat pores and ridge contours (level 3), thereby offering clear and compelling evidence for personal identification and demonstrating the effectiveness of this approach for LFP recognition. Based on their fluorescence emission spectra and chromaticity diagram, the developed contrast was quantified using eqn (1)–(3).[23]

$$I = \frac{S_A}{S_B} \tag{1}$$

$$C = \frac{|AB|}{|AP|} = \frac{\sqrt{(X_B - X_A)^2 + (Y_B - Y_A)^2}}{\sqrt{(X_P - X_A)^2 + (Y_P - Y_A)^2}} \tag{2}$$

$$\text{Contrast} = C \log I \tag{3}$$

here, I represents the intensity index, and C denotes the chroma index. A, B, and P correspond to the LFP developed using the probe, the blank substrate, and the pure probe, respectively. The intensity index was determined from the integrated area under the fluorescence emission peak of each sample, while the chroma index was calculated based on the color difference between the developed fingerprint signal and the background noise in the chromaticity diagram (Fig. S19a and b). The calculated intensity index for LFP development using *p*-TPyMe was 4.84, indicating that the fingerprint signal is approximately five times brighter than the background. Furthermore, the chroma index was calculated to be 7.87, highlighting a significant color contrast between the developed fingerprint pattern and the background. Therefore, the fingerprint developed using the water-soluble *p*-TPyMe on aluminium foil exhibited a contrast value of 5.39, markedly higher than commonly reported values, ensuring distinct ridge-to-valley separation crucial for reliable forensic interpretation.

To assess the practical applicability of the *p*-TPyMe probe, LFP development was carried out on a range of substrates, including aluminum foil, glass, coin, tin foil, plastic, steel, and adhesive tape (Fig. 5b). LFP development can be achieved using different methods, among which the soaking method offers several practical advantages. This approach eliminates the need for post-treatment, enabling convenient on-site operation. It is particularly advantageous for water-resistant materials such as tinfoil, steel, glass, and plastic, as the dye solution covers surfaces evenly, ensuring high-resolution images. Additionally, the soaking method is characterized by safety, cleanliness, ease of storage, economical operation, user-friendliness, and high efficiency, making it a practical and convenient technique for LFP

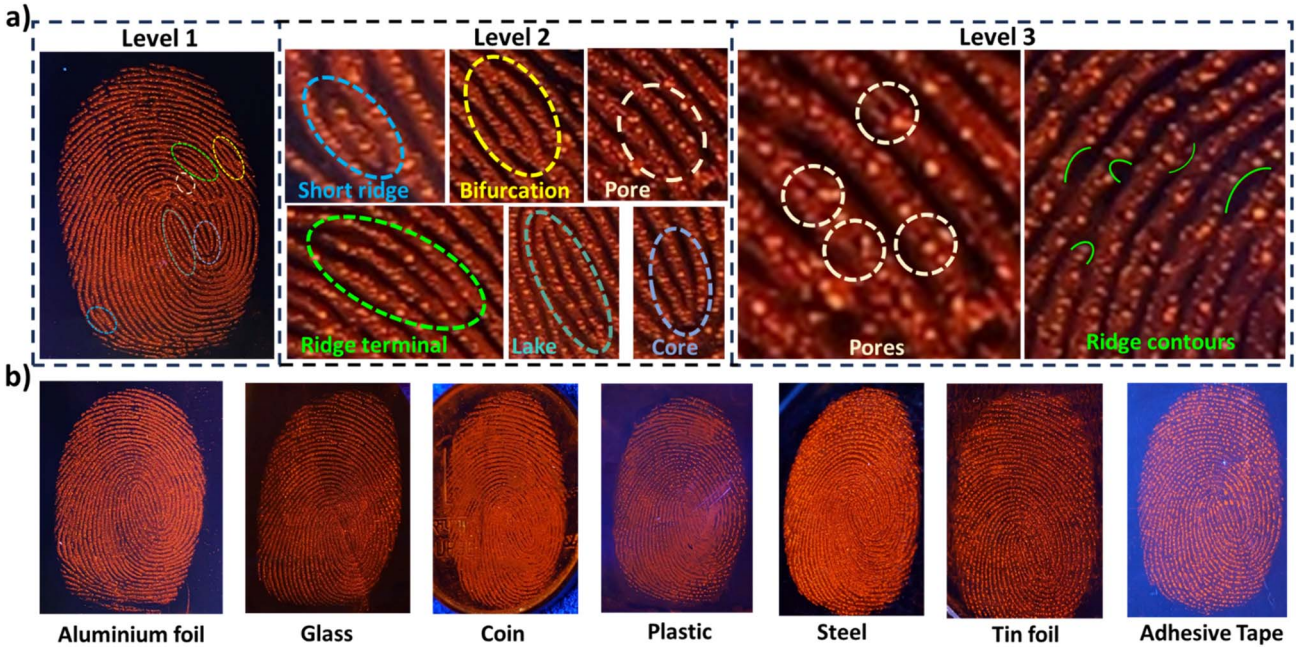

Fig. 5 (a) Fluorescence microscopic images of LFPs developed on aluminium foil, revealing level 1 (overall ridge pattern and core), level 2 (ridge terminal, bifurcations, lake), and level 3 (ridge edge contours, sweat pore distribution) details. (b) Digital images of latent fingerprints developed using *p*-TPyMe (50 μM) on various substrates, including aluminum foil, glass, coin, plastic, stainless steel, tin foil, and adhesive tape under 365 nm UV illumination.

development in various scenarios. The development of LFPs on various substrates were obtained *via* the soaking method using a 50 μM aqueous solution of *p*-TPyMe yielded distinct fingerprint patterns with excellent contrast and resolution (Fig. 5b). LFPs can also be collected from curved surfaces such as spoons, plastic caps, cups, and steel tubes (Fig. S19c and d). However, capturing a clear and complete fingerprint image is difficult because the camera struggles to focus on the entire print on these curved surfaces. Fingerprint identification at a crime scene often involves detecting LFPs that have remained on surfaces for a long time. To verify the potential of *p*-TPyMe probe, a series of aged LFPs on aluminium foil were treated and analysed. As depicted in Fig. S20a, the LFPs aged for 1, 3, 7, 15, and 30 days were developed exceptionally well, resulting in sharp, high-resolution images that clearly displayed even level 3 details. TGA and fluorescence thermal stability analysis revealed that the emission behavior of the compound remains stable up to 100 °C (Fig. S17d and 20b). Thus, this probe holds great promise for enhancing on-site fingerprint collection, providing a practical and reliable solution for comprehensive LFP analysis to advance standardized forensic protocols.

Conclusions

In summary, we have designed a series of AIE-active positional isomers based on a D–A–A′ framework, *p*-TPy, *m*-TPy, and *o*-TPy by altering the position of the pyridine ring with respect to the malononitrile group within the acceptor unit, aiming to investigate the structure–property relationships among the isomers. Upon shifting the position of the pyridine group from *para* to *ortho*, the molecular configuration was notably altered, resulting in variations in the electron-accepting ability of the acceptor unit and influencing the molecular packing of the isomers within the crystal lattice. These structural modifications, in turn, modulated their photophysical properties, as reflected in their solid-state emission maxima, which progressively red-shifted from 560 nm to 580 nm to 612 nm, with corresponding quantum yields of 0.16, 0.49, and 0.44 for *p*-, *m*-, and *o*-TPy, respectively. A detailed comparative study of the isomers was performed, assessing their AIE characteristics, solvatochromism, and transient PL, supported by single-crystal X-ray diffraction and theoretical calculations. In addition, the *para* isomer, *p*-TPy, served as the key ingredient in crafting a TLM by embedding it within a phase-changing PEG matrix. By incorporating *p*-TPy into PEG matrices of different molecular weights, PEG2000, PEG4000, and PEG20000, three distinct TLM-based security inks were developed, each displaying a distinct color-changing response at different temperatures. This innovative approach enables the creation of security inks with precisely tuned thermal behaviors, significantly enhancing their effectiveness for sophisticated, multi-level data encryption and authentication applications. Leveraging the nucleophilic character of the pyridine nitrogen in the *para* isomer (*p*-TPy), a methylation reaction was strategically employed to form a pyridinium salt, yielding a water-soluble, amphiphilic emitter (*p*-TPyMe). This structural transformation was specifically designed to enhance performances in latent fingerprint detection applications. The resulting fluorophore offered effective LFP visualization through a fluorescence "off–on" mechanism at longer emission wavelengths, achievable by a simple immersion method with an aqueous *p*-TPyMe solution, without

the involvement of organic cosolvents or further post-treatment. The effectiveness of LFP detection was assessed on a wide range of surfaces, ranging from aluminium and tin foils to stainless steel, glass, coins, adhesive tape, and plastics. Not only does it clearly reveal the fundamental level 1 fingerprint patterns, but it also enables precise identification of level 2 and level 3 details, such as ridge endings, bifurcations, short ridges, and even minute pores. This is achieved through its impressive contrast value of 5.39 against the background, thereby facilitating highly accurate forensic analysis. Thus, this approach holds great promise for enhancing on-site fingerprint detection, offering a robust and versatile tool to advance standardized forensic protocols. The outcomes of this research establish a clear structure–property correlation in positional isomers and demonstrate the successful translation of molecular design into practical thermochromic security inks and high-performance fingerprint detection agents, thereby driving innovations at the molecular engineering level interfacing material chemistry, security encryption technologies and forensic science.

Author contributions

The manuscript was written through the contributions of all authors. Credit: DB conceptualized and designed the project, synthesized all the probes, conducted the experiments, performed computational calculations and data analysis, and drafted the manuscript. RP contributed to data collection, analysis, and manuscript revisions. PKI supervised the project, secured funding, and was actively involved in project planning, data interpretation, manuscript preparation, and revisions. All authors approve the final version of the manuscript.

Conflicts of interest

There are no conflicts to declare.

Data availability

The data supporting this article have been included as part of the supplementary information (SI). Supplementary information: experimental details, characterization data (NMR, HRMS, UV, PL, FESEM, SCXRD, PXRD, DFT). See DOI: https://doi.org/10.1039/d5sc08281a.

CCDC 2451454 and 2451455 contain the supplementary crystallographic data for this paper.[24a,b]

Acknowledgements

The authors thank DST-India (No. DST/SERB/EMR/2014/000034), DST/CRG/2019/002164, DeitY-India Project No. 5(1)/2022-NANO, ICMR, Grant No. 5/3/8/20/2019-ITR and DST-Max Planck Society, Germany (No. IGSTC/MPG/PG(PKI)/2011A/48) for financial support. The Department of Chemistry (FIST: SR/FST/CS-II/2017/23C), Centre for Nanotechnology and Central Instruments Facility, IIT Guwahati, are acknowledged for providing instrument facilities. D. B. thanks MHRD for the Fellowship. The authors gratefully acknowledge Soumalya Bhowmik for assisting in image acquisition studies.

Notes and references

1 N. Akshaya, A. Thomas, G. J. Martis and S. L. Gaonkar, Recent advances in organic fluorophores as anti-counterfeit agents: an up-to-date review, *Discov. Appl. Sci.*, 2025, **7**, 110.
2 A. H. Malik, A. Kalita and P. K. Iyer, Development of Well-Preserved, Substrate-Versatile Latent Fingerprints by Aggregation-Induced Enhanced Emission-Active Conjugated Polyelectrolyte, *ACS Appl. Mater. Interfaces*, 2017, **9**, 37501–37508.
3 B. Daly, J. Ling and A. P. de Silva, Current developments in fluorescent PET (photoinduced electron transfer) sensors and switches, *Chem. Soc. Rev.*, 2015, **44**, 4203–4211.
4 R. Kumar, A. Sharma, H. Singh, P. Suating, H. S. Kim, K. Sunwoo, I. Shim, B. C. Gibb and J. S. Kim, Revisiting Fluorescent Calixarenes: From Molecular Sensors to Smart Materials, *Chem. Rev.*, 2019, **119**, 9657–9721.
5 J. Luo, Z. Xie, J. W. Y. Lam, L. Cheng, H. Chen, C. Qiu, H. S. Kwok, X. Zhan, Y. Liu, D. Zhu and B. Z. Tang, Aggregation-induced emission of 1-methyl-1,2,3,4,5-pentaphenylsilole, *Chem. Commun.*, 2001, 1740–1741.
6 M. Echeverri, C. Ruiz, S. Gámez-Valenzuela, M. Alonso-Navarro, E. Gutierrez-Puebla, J. L. Serrano, M. C. Ruiz Delgado and B. Gómez-Lor, Stimuli-Responsive Benzothiadiazole Derivative as a Dopant for Rewritable Polymer Blends, *ACS Appl. Mater. Interfaces*, 2020, **12**, 10929–10937.
7 Q. Wang, Q. Zhang, Q.-W. Zhang, X. Li, C.-X. Zhao, T.-Y. Xu, D.-H. Qu and H. Tian, Color-tunable single-fluorophore supramolecular system with assembly-encoded emission, *Nat. Commun.*, 2020, **11**, 158.
8 W. Zhong, J. Zhang, Y. Lin, S. Li, Y. Yang, W.-J. Wang, C. Si, F. E. Kühn, Z. Zhao, X.-M. Cai and B. Z. Tang, Multi-site isomerization of synergistically regulated stimuli-responsive AIE materials toward multi-level decryption, *Chem. Sci.*, 2024, **15**, 3920–3927.
9 X.-M. Cai, Y. Lin, J. Zhang, Y. Li, Z. Tang, X. Zhang, Y. Jia, W. Wang, S. Huang, P. Alam, Z. Zhao and B. Z. Tang, Chromene-based BioAIEgens: 'in-water' synthesis, regiostructure-dependent fluorescence and ER-specific imaging, *Natl. Sci. Rev.*, 2023, **10**, nwad233.
10 N. Meher, A. P. Bidkar, D. Barman, S. S. Ghosh and P. K. Iyer, A conformational tweak for enhanced cellular internalization, photobleaching resistance and prolonged imaging efficacy, *Chem. Commun.*, 2020, **56**, 14861–14864.
11 W. Zhu, Y. Li, S. Guo, W.-J. Guo, T. Peng, H. Li, B. Liu, H.-Q. Peng and B. Z. Tang, Stereoisomeric engineering of aggregation-induced emission photosensitizers towards fungal killing, *Nat. Commun.*, 2022, **13**, 7046.
12 W. Zhong, Y. Wu, Y. Lin, S. Li, J. Zhang and X.-M. Cai, Fabrication of efficient and red-emissive salicylaldehyde Schiff base isomers for multi-scenario information decryption, *J. Mater. Chem. C*, 2024, **12**, 11394–11401.

13 X.-M. Cai, S. Li, W.-J. Wang, Y. Lin, W. Zhong, Y. Yang, F. E. Kühn, Y. Li, Z. Zhao and B. Z. Tang, Natural Acceptor of Coumarin-Isomerized Red-Emissive BioAIEgen for Monitoring Cu2+ Concentration in Live Cells via FLIM, *Adv. Sci.*, 2024, **11**, 2307078.

14 G. Fan and D. Yan, Positional isomers of cyanostilbene: two-component molecular assembly and multiple-stimuli responsive luminescence, *Sci. Rep.*, 2014, **4**, 4933.

15 L. R. Adil and P. K. Iyer, Effects of incorporating regioisomers and flexible rotors to direct aggregation induced emission to achieve stimuli-responsive luminogens, security inks and chemical warfare agent sensors, *Chem. Commun.*, 2020, **56**, 7633–7636.

16 B. Roy, I. Maisuls, J. Zhang, F. C. Niemeyer, F. Rizzo, C. Wölper, C. G. Daniliuc, B. Z. Tang, C. A. Strassert and J. Voskuhl, Mapping the Regioisomeric Space and Visible Color Range of Purely Organic Dual Emitters with Ultralong Phosphorescence Components: From Violet to Red Towards Pure White Light, *Angew. Chem., Int. Ed.*, 2022, **61**, e202111805.

17 H.-T. Feng, J. Zeng, P.-A. Yin, X.-D. Wang, Q. Peng, Z. Zhao, J. W. Y. Lam and B. Z. Tang, Tuning molecular emission of organic emitters from fluorescence to phosphorescence through push-pull electronic effects, *Nat. Commun.*, 2020, **11**, 2617.

18 K. Jiang, Y. Wang, C. Cai and H. Lin, Conversion of Carbon Dots from Fluorescence to Ultralong Room-Temperature Phosphorescence by Heating for Security Applications, *Adv. Mater.*, 2018, **30**, 1800783.

19 Y. Ma, Y. Yu, P. She, J. Lu, S. Liu, W. Huang and Q. Zhao, On-demand regulation of photochromic behavior through various counterions for high-level security printing, *Sci. Adv.*, 2020, **6**, eaaz2386.

20 J. Mei, N. L. C. Leung, R. T. K. Kwok, J. W. Y. Lam and B. Z. Tang, Aggregation-Induced Emission: Together We Shine, United We Soar, *Chem. Rev.*, 2015, **115**, 11718–11940.

21 Y.-L. Wang, C. Li, H.-Q. Qu, C. Fan, P.-J. Zhao, R. Tian and M.-Q. Zhu, Real-Time Fluorescence In Situ Visualization of Latent Fingerprints Exceeding Level 3 Details Based on Aggregation-Induced Emission, *J. Am. Chem. Soc.*, 2020, **142**, 7497–7505.

22 J. Jiang, D. Hu, M. Hanif, X. Li, S. Su, Z. Xie, L. Liu, S. Zhang, B. Yang and Y. Ma, Twist Angle and Rotation Freedom Effects on Luminescent Donor–Acceptor Materials: Crystal Structures, Photophysical Properties, and OLED Application, *Adv. Opt. Mater.*, 2016, **4**, 2109–2118.

23 M. Wang, D. Shen, Z. Zhu, M. Li, C. Yuan, Y. Zhu, J. Wu and C. Mao, Quantifying contrast of latent fingerprints developed by fluorescent nanomaterials based on spectral analysis, *Talanta*, 2021, **231**, 122138.

24 (*a*) CCDC 2451454: Experimental Crystal Structure Determination, 2026, DOI: 10.5517/ccdc.csd.cc2n8y52; (*b*) CCDC 2451455: Experimental Crystal Structure Determination, 2026, DOI: 10.5517/ccdc.csd.cc2n8y63.